Journal of Materials Chemistry C

As Good as Gold and Better: Conducting metal oxide materials for mid-infrared plasmonic applications

Journal:	*Journal of Materials Chemistry C*
Manuscript ID	TC-REV-12-2017-005760.R1
Article Type:	Review Article
Date Submitted by the Author:	30-Jun-2018
Complete List of Authors:	Khamh, Hniang; North Carolina State University, Chemistry Sachet, Edward; North Carolina State University, Materials Science and Engineering Kelley, Kyle; North Carolina State University, Materials Science and Engineering Maria, J. P.; North Carolina State University, Materials Franzen, Stefan; North Carolina State University, Chemistry

As Good as Gold and Better:

Conducting metal oxide materials for mid-infrared plasmonic applications

Hniang Khamh[1], Edward Sachet[2], Kyle Kelly[2], Jon-Paul Maria[2], Stefan Franzen[1]

1. Department of Chemistry, North Carolina State University, Raleigh, NC 27695
2. Department of Materials Science and Engineering, North Carolina State University, Raleigh, NC 27695

Abstract

The field of infrared surface plasmon resonance (IR-SPR) spectroscopy has the potential to enable unique applications and technologies in chemical sensing, heat harvesting, and infrared detectors. Finding an ideal material that can support a surface plasmon in the IR region has been a challenge for more than a decade. High carrier mobility, $\mu > 200 \frac{cm^2}{Vs}$, and tunable carrier concentration in the range $10^{19} < n < 10^{21}$ cm^{-3} are two necessary criteria for a spectrally narrow tunable plasmon resonance band in the IR. The ideal material would also be easy to prepare and robust in water and under ambient conditions. In this review, we highlight the development of the field over the last decade. We also provide a guide to explain the extension of visible plasmonics to the infrared region and the evolution of IR-SPR using conducting metal oxides (CMOs). CMOs are free electron conductors and most of them have no interfering electronic or vibrational transitions in the range of interest. Therefore, these materials also provide an excellent test of the fundamental physics of SPR, including the effects of surface fields, enhancement phenomena and the relationship between thin film epsilon near zero (ENZ) mode and the localized surface plasmon resonance (LSPR) in nanocrystals. In summary, we discuss the materials challenges and prospects for this field of research.

1. Introduction

Since the emergence of the field of surface plasmon resonance (SPR) spectroscopy in the 1950's, the SPR technique has been developed primarily employing the noble metals Au and Ag because of the accessibility of resonances in the visible region of the electromagnetic spectrum in these metals.[1] The idea of extending the SPR phenomenon to new materials and to the infrared (IR) region in the wavelength range from 1 to 10 microns has only been explored during the past decade.[2-4] Fundamentally, the physics of SPR does not change in the IR compared to the visible region, but the materials requirements are dramatically different. The optical resonances in Au and Ag can be tuned by changing the size and shape of colloids and nanoscale surface structures, but the charge carrier density and mobility are fixed material properties in metals. As radiation is tuned further from resonance with the bulk plasmon of Ag and Au, the losses in these materials increase dramatically. Consequently, IR applications require new materials. The concept of a tunable surface plasmon in a free electron conductor was introduced with the suggestion that semiconductors can serve as tunable materials in the infrared region for SPR applications.[5, 6] Research efforts in the past decade have shown that there are numerous conducting metal oxides (CMOs) that have an appropriate carrier density to support SPR in the mid-IR region.[6-8] However, the crucial property of a useful SPR material is a sufficiently large free carrier mobility to permit a high quality factor, i.e. a narrow, sharp SPR band.[9]

For many years ITO has been the workhorse in the field of near-IR SPR spectroscopy. Using indium tin oxide (ITO), it was possible to systematically determine the effect of material parameters and thin film preparation on the SPR response.[10, 11] Although ITO is a versatile material for demonstrating the range of possible effects in the near-IR (from 1-2 microns), it is far from the ideal SPR material for IR applications because of its low mobility (< 30 cm^2/Vs). ITO has typically high defect concentrations since the doping level of Sn is relatively high (ca. 10%) in standard thin film preparations. In practice, the SPR in ITO is much broader than in Au and there appears to be no feasible way to produce a thin film of ITO with sufficiently high free carrier mobility to overcome this limitation.[10, 11]

There are many CMOs to consider that may have a desirable combination of free carrier density and mobility appropriate for mid-IR SPR applications. Doped ZnO has been investigated because it is robust material, inexpensive and supports lower doping levels than ITO.[5, 12-14] ZnO

can be doped with Al, Ga or other ions at lower concentrations than tin in ITO to achieve conducting thin films with free carrier densities appropriate for mid-IR applications. However, the mobility of ZnO films is also low and the SPR is correspondingly broad. There have been a few studies on other oxides, e.g. strontium ruthenate, which have similar limitations. The studies of a variety of CMOs leads to the conclusion that the starting point for design of a new material is to identify a CMO that has a high mobility. It has long been known that CdO has high mobility, but the appropriate doped CMO films for mid-IR applications were not known until recently.[9]

In 2015 dysprosium-doped cadmium oxide (CdO:Dy) was demonstrated as a gateway material that can support narrow, high quality SPR in the mid-IR region.[9] Based on this work, we will address the interplay of theory and experiment involved in the extension of SPR from visible to infrared region, theory of SPR technique, and the evolution of CMO materials that has been developed for IR-SPR, and the future of IR-SPR using CMOs and their possible applications. The development of SPR in thin film materials has been complemented by studies of localized surface plasmon resonance (LSPR) in nanoparticles and nanostructures.[15-17] While the geometries differ, both SPR and LSPR depends on the inherent transport properties of a material to support a surface plasmon polariton (SPP), which is a consequence of the natural resonant frequency in the material due to free charge carriers. Electromagnetic radiation can drive a resonance in the material, but that effect is dependent upon the angle of incidence in a thin film (SPR) or the geometry of a nanostructure (LSPR), both of which affect the conservation of momentum of the absorbed photons. The development of mid-IR LSPR in parallel to thin film SPR provides complementary information on the materials and their possible applications. We will give the theoretical and experimental background that has motivated the focus on CMOs as the most promising materials for mid-IR plasmonic applications. Finally, we will discuss connection between the epsilon-near-zero (ENZ) mode and the LSPR in our brief review of the theoretical background of the observed optical properties of thin films and nanostructures in the mid-IR.

1.1.The Drude Model for optical properties of Conducting Metal Oxides

A plasmon resonance that can be described using the free electron (Drude) model can be called a “pure plasmon”. The Drude model was constructed to explain the transport properties of

conduction electrons in an ideal material. It has been applied to conductivity in metals, conductive oxides and heavily doped semiconductors despite the fact that there is a significant departure from ideal behavior in many of these materials. For example, the Drude model cannot capture the optical effects of interband transitions of the noble metals, Au and Ag, in the visible and near-IR. The model is applicable to most CMOs provided their bandgaps are sufficiently high. The CMOs of interest are transparent in the visible region or colored reddish or orange with band gaps range from 2-3 eV. The observed ENZ in these materials ranges from 0.2-1.0 eV. The bandgap energy is significantly greater than the plasmon band energy in all of these materials. Thus, the difference in energy between bandgap transitions and the optical resonances due to plasmons is quite large. Provided there are no interband transitions, the Drude model accurately describes the optical properties of a CMO based on the equation of motion of an electron in a field of nuclei with three adjustable parameters. The dielectric function of a conductor can be described using Drude model as follows:

$$\varepsilon_m = \varepsilon_1 - i\varepsilon_2 = \varepsilon_\infty - \frac{{\omega_p}^2}{\omega^2 + i\gamma\omega} \tag{1.1}$$

The real and imaginary dielectric function can be separated as:

$$\varepsilon_1 = \varepsilon_\infty - \frac{{\omega_p}^2}{\omega^2 + \gamma^2} \tag{1.2}$$

$$\varepsilon_2 = \frac{{\omega_p}^2 \gamma}{\omega^3 + \omega\gamma^2} \tag{1.3}$$

The plasma frequency and damping constant can be described by:

$$\omega_p = \sqrt{\frac{nq^2}{m_e \varepsilon_0}} \tag{1.4}$$

$$\gamma = \frac{q}{\mu m_{eff}} \tag{1.5}$$

ε_m dielectric function

ε_∞ high frequency limit

γ damping constant

ω_p plasma frequency

n carrier density

q electron charge

ε_0 the permittivity of vacuum

m_{eff} effective electron mass

μ mobility

The first parameter is the charge carrier density, *n*. CMO carrier densities in the range of interest for IR applications (10^{19} –10^{21} cm^{-3}) are two to four orders of magnitude lower than those of noble metals (ca. 10^{23} cm^{-3}). As given in equation (1.3), the plasma frequency is proportional to the square root of the carrier density. The free electron model has proven very accurate for describing the mid- and near infrared portion of the spectrum, which covers the optical properties of these semiconductors in the range from 1,000 – 10,000 cm^{-1}. The longer wavelengths used to drive SPR in CMOs have consequences for the spatial extent of plasmonic fields as well as the thickness of metal oxide thin films required for the effect to be observed.

The second phenomenological parameter in the Drude model is the damping, γ. The damping in plasmonic spectroscopy plays a similar role to the dephasing rate in optical spectroscopy. An increase in damping results in a spectrally broader plasmon. This parameter turns out to be of crucial interest for applications since the spectral bandwidth of the plasmonic resonance determines its utility for nearly every application of interest. In metals there is no practical way to tune the damping, but it is sufficiently low for the noble metals that useful SPR effects can be observed in the UV-VIS. CMOs present a pronounced variability in γ owing to the two material parameters that comprise the damping, the mobility (μ) and the effective mass (m_{eff}), whose relationships are given in equation (1.5). Equation 1.3 shows that the loss (ε_2) is roughly proportional to γ. The effective mass is a property governed by the band structure of the CMO and can be considered a material constant. The high frequency dielectric constant (ε_∞) is a parameter that depends on the degree of screening of the lattice by the electron distribution in the solid. The distribution is a property of the material and it is difficult to imagine that there will be opportunities to significantly engineer this parameter.

The Drude model is a simple yet effective model that permits us to predict the dielectric properties in the frequency band of interest for any CMO using only four material parameters: carrier concentration, mobility, effective mass of the free carrier and high frequency dielectric constant. Two of the material parameters simultaneously affect the phenomenological damping, which reduces the number of parameters in the basic Drude theory to three. From the perspective of material design, we will show that by far the most important two parameters are n and μ. n controls the wave number of the surface plasmon band and μ is the material parameter that can be engineered to enhance plasmonic performance by tuning the spectral bandwidth. One can relate the mobility to the degree of scattering of electrons by the lattice and carrier screening. Lattice defects, such as grain boundaries increase scattering and reduce performance.

A dielectric function of a generic Drude material with a given value for n, μ, m_{eff} and ε_∞ can be plotted as depicted in Figure 1. ε_1 (solid) and ε_2 (dashed) are the real and the imaginary components of the dielectric function, respectively. ε_1 decreases steadily as the energy decreases while ε_2 exhibits the opposite trend. As frequency is lowered the real part $\varepsilon_1$changes sign from positive to negative at a frequency known as the epsilon-near-zero (ENZ) frequency, then falls steeply below this value. The ENZ frequency is of interest in its own right because of the fact that a thin film can absorb all of the energy in an incident electromagnetic wave at this frequency.[18-20] The region just below the ENZ frequency comprises the range of interest for IR-SPR since plasmonic oscillation can only be supported if $\varepsilon_1 < 0$. The imaginary component ε_2, also called the loss tangent, approaches zero at high frequency (1.3). ε_2 increases as the frequency is lowered with a hyperbolic frequency dependence becoming significant for energies where ε_1 becomes negative. Recognition of the nature of the requirements for observation of SPR in terms of ε_1 and ε_2 defines the challenge for development of a robust material that can support SPR in the infrared region in terms of material properties that can be controlled by experimental conditions.

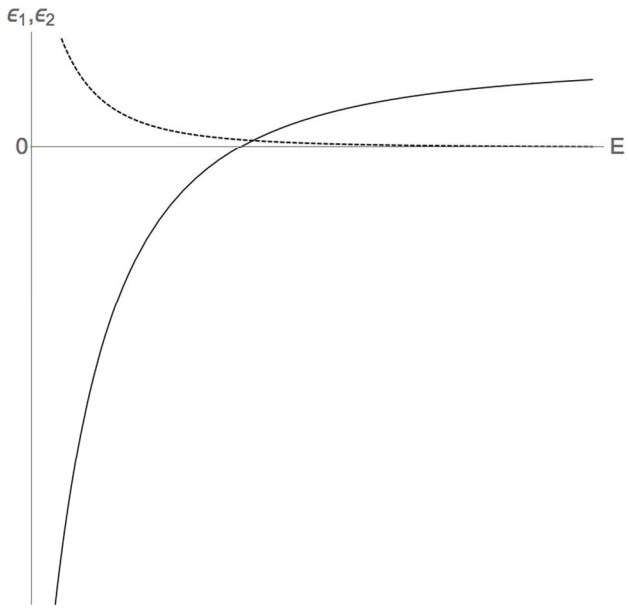

Figure 1. Example plot of Drude model dielectric: The real part (solid) and the imaginary part (dash) plotted as a function of energy.[21]

1.2.The effects of material property variables in the Drude model

The effect of four parameters, n, μ, m_{eff} and ε_∞ can be considered independently to fully understand how the Drude model depends on material properties. We can further differentiate between parameters that are dependent on the preparation conditions, which are n and μ, and those that are dependent on chemical composition, which are m_{eff} and ε_∞. Keeping this distinction in mind, we will discuss the general considerations of all four parameters.

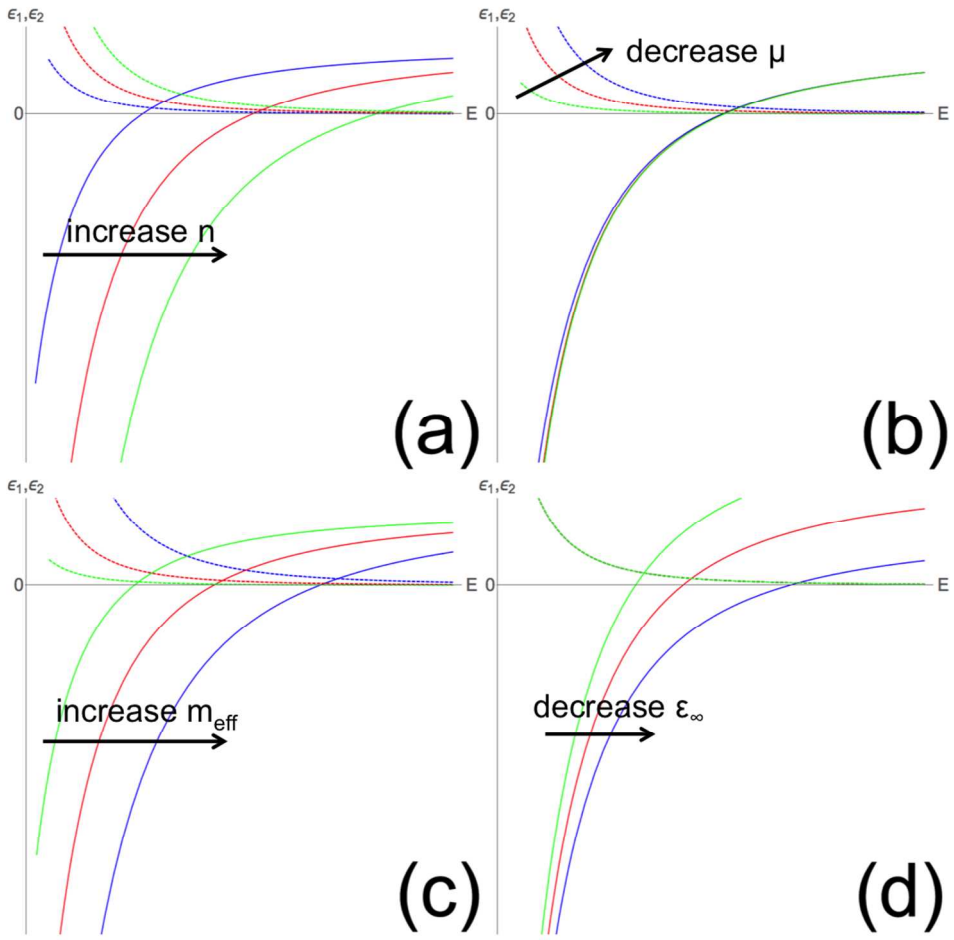

Figure 2. The effect of varying the input parameters *n*, μ, m_{eff} and ε_∞on the calculated Drude dielectric functions. The effect of increasing (a) carrier concentration *n* (b) mobility μ (c) effective electron mass m_{eff} (d) high frequency dielectric constant ε_∞, while keeping the remaining properties constant.[21]

Increasing the carrier concentration *n* results in shifting the ENZ frequency to a higher energy as shown in Figure 2a. The ENZ is observed at the point where ε_1 crosses zero, which is also called the cross-over frequency. This is one of the advantages of using semiconductors since the ENZ frequency can be tuned by varying the carrier concentration via doping. Increasing the mobility, μ, on the other hand does not affect the cross-over of frequency of ε_1 but strongly reduces the loss tangent ε_2 (Figure 2b). The inverse correlation of mobility and loss tangent is largely independent of the free carrier concentration. Figure 2c depicts the result of varying effective electron mass. As given in equation 1.4, the plasma frequency is directly proportional to square

root of the ratio of the carrier concentration to the effective electron mass $m_{eff} = \rho m_e$, where m_e is the electron mass and ρ is a screening parameter. The effect of decreasing effective mass is to increase the carrier concentration; both the ENZ mode and the SPP shift to higher frequency (wave number). Although a reduction in the effective mass increases the damping constant, γ, and correspondingly the loss function ε_2, this effect is not nearly as important as that of the mobility. The range of m_{eff} values from $0.25m_e < m_{eff} < 0.75m_e$ is roughly a factor of three, while mobility has a much greater range of values in practice $10 < \mu < 500\ cm^2/Vs$ spanning at least a factor of 50. Of course, it crucial that m_{eff} is an inherent parameter that changes little with film preparation, while μ can vary widely depending on sputtering and annealing conditions. In general, we have shown that μ decreases as the lattice imperfections increase. [11] These imperfections may be caused by doping itself, which can disrupt the lattice or by deposition conditions which affects the grain size and consequently the scattering length of conduction electrons. Often there is an inverse relationship between *n* and μ since increasing the density of free carriers by doping often increases the concentration of lattice imperfections due to the mismatch in the radius of the dopant in relation to the original ion that was replaced. However, we have also shown that the defect equilibrium is fixed in some materials due to entropic effects, which means that compensating structural changes may occur that actually reduce lattice imperfections caused by doping. The net effect of this fortuitous cancellation is that *n* and μ can both increase over certain ranges.[9] Although this effect has only recently been discovered based on the work on CdO:M (M = Dy, Y, F), there is reason to believe that it is a general effect in some classes of materials and may be important for the engineering of new materials.

Finally, increasing the high frequency dielectric constant ε_∞, shifts the ENZ frequency to a higher energy without affecting the loss tangent ε_2. Increasing ε_∞ increases the curvature of the real part of the dielectric function, ε_1, and consequently lowers the ENZ. Understanding the effect of these input parameters for Drude model is essential in optimizing host materials for plasmonic applications. Appropriate choice of host oxide materials permits one to obtain the correct range for m_{eff} and ε_∞. Selection of appropriate dopants, deposition and annealing conditions permits control of *n* and μ to fine tune the optical properties. Appropriate experience and understanding of the theory permits prediction of material properties in advance of film

preparation. The example of the correlation of n and μ due to the defect equilibrium also focuses our attention on the fact that the parameters are not always independent. At present, these correlations are sufficiently well understood to permit the design of tailor-made thin film materials with SPR resonances in the mid-IR from 800 – 5000 cm^{-1} and sufficiently high mobility for sensing and spectroscopic applications.

1.3. Experimental observation of the SPR phenomenon

In order to understand the various coupling schemes for surface plasmon resonance we begin with the derivation from a model comprised of a thin metal film and a dielectric. In the Drude model, it is assumed that motionless positive ions in the conductor are surrounded by a non-interacting electron gas.[22] As for the dielectric, a non-dispersive medium is assumed. This section is based on a reduced form of the Drude model, which permits useful comparisons for understanding the role of various parameters.[21] In a lossless Drude metal given in eq 1.1, $\gamma = 0$. Assuming $\varepsilon_\infty = 1$ and $\Omega = \frac{\omega}{\omega_p}$, the lossless frequency dependent dielectric function (eq 1.1) can be expressed as:

$$\varepsilon_{Drude} = (1 - \frac{1}{\Omega^2}) \tag{1.6}$$

The dispersion relation that allow SPP to propagate in any model is given by

$$k_{SPP} = \frac{\omega}{c}\sqrt{\frac{\varepsilon_0 \varepsilon_s}{\varepsilon_0 + \varepsilon_s}} \tag{1.7}$$

ω represents the angular frequency, c is the speed of light. ε_0 and ε_s represent the dielectric functions of the insulating overlayer (ε_0) and conducting substrate (ε_s), respectively. Setting $\varepsilon_0 = 1$, combining equations 1.6 and 1.7, and normalizing all energies to ω_p using equations 1.8 and 1.9 give:

$$K = \frac{k}{k_p} \tag{1.8}$$

$$k_p = \frac{\omega_p}{c} \tag{1.9}$$

$$K = \sqrt{\frac{\Omega^2 - 1}{2\Omega^2 - 1}} . \Omega \quad (1.10)$$

Plotting equation 1.10 yields two distinct curves as shown in Figure 4a. The upper branch describes the oscillation of the bulk plasmon in the metallic material and known as bulk plasmon polariton (BPP). The lower branch is the dispersion curve of surface plasmon polaritons (SPP). BPP are excited at frequencies higher than the plasma frequency ($\omega > \omega_{bp}$) while SPP are excited at $\omega < \omega_{bp}$. SPPs are bound electromagnetic density waves that oscillate and propagate parallel to conductor/dielectric interfaces. The upper limit of the energy gap between SPPs and BPPs found to be equal to the plasma frequency ω_p.

The dispersion relation of light in an isotropic medium, commonly known as a *light line*, in energy-wavevector space can be summarized for a medium with ε = 1 as:

$$k_{light} = \frac{\omega_{light}}{c} \quad (1.11)$$

The light line and SPP plotted together are shown in Figure 3b. Note that the light line does not intersect with the dispersion curve of the SPP at any point of the curve for electromagnetic radiation propagating in vacuum (or air). This implies that light propagating through a medium with ε = 1 cannot couple to SPPs and drive the SPR under these conditions since the in-plane momentum of the wave vector of SPPs is always larger than the momentum of the incoming light. For SPPs and the light to couple and drive SPR, the momentum of the light needs to be increased. To solve this problem Kretschman and Raether proposed the Kretschman[23, 24]-Reather configuration[25] (Kretschman configuration for short). At the same time, Otto[26] presented an alternative approach to excite the plasmons in the metal surface shown in Figures 3a and 3b respectively. The alternative method is called the Otto configuration. Both configurations use a prism as a propagating medium to increase the in-plane momentum of the incident light.

By incorporating prism into light line equation, assuming a lossless dielectric medium ε_D can be written as:

$$k_{light} = \frac{\omega_{light} \cdot \sqrt{\varepsilon_D}}{c} \quad (1.12)$$

Plotting this equation, one can see that the light line now intersects with the dispersion curve of the SPP (Fig. 3c).

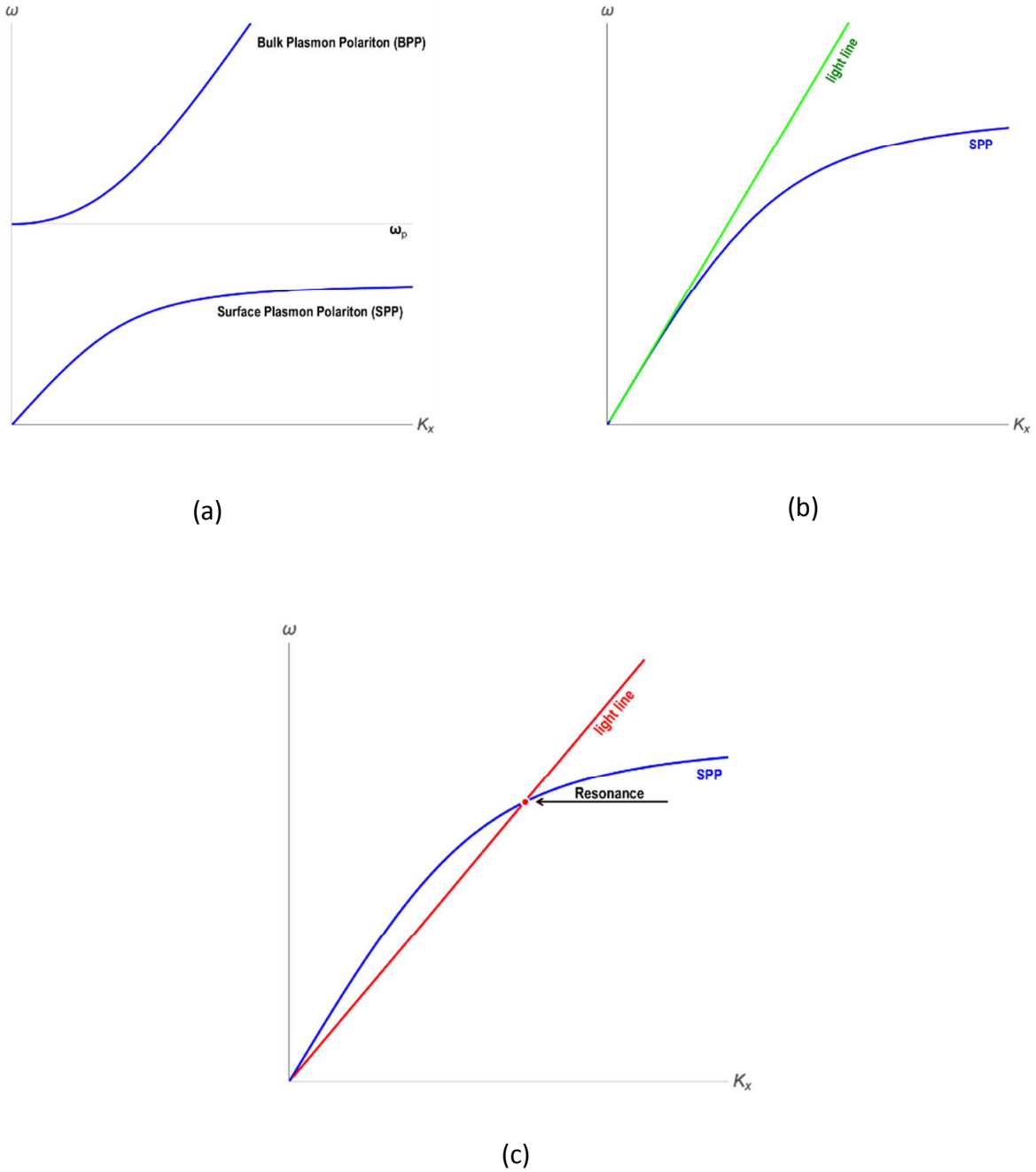

Figure 3. The dispersion curves as calculated using the Drude model and coupling of EM waves with SPP. (a) the dispersive curve of BPP and SPP describe by Drude model in a metallic thin film. (b) SPP dispersive curve with in a medium with epsilon = 1. (c) SPP dispersive curve

coupling to light by increasing the momentum of the incoming photons by using an optically dense (ε > 1) prism.[21]

$$k_{(x)light} = \frac{\omega_{light} \cdot \sqrt{\varepsilon_D} . \sin(\theta_i)}{c} \quad (1.13)$$

The total internal reflection method is used in both Kretschman and Otto configurations. The incoming light k_x propagates through the prism and an evanescent field is created by total internal reflection. The coupling occurs when the momentum of this incoming light matches the SPP dispersion. This phenomenon is known as *surface plasmon resonance* (SPR). In this experiment, the in-plane wavevector of the incoming light can be varied by changing the angle of the incoming light. If we include this angle variation of incident light, the modified equation is given in eq 1.13. Plotting this equation for various angles with a SPPs dispersion indicates how different angles give different resonance points (thus combinations of k_x and energy) on the SPP dispersion curve.

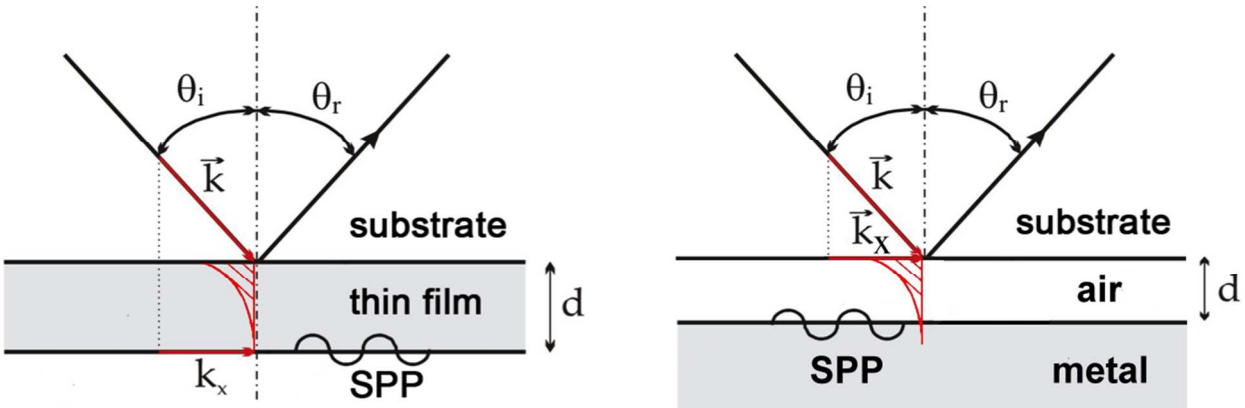

Figure 4. Schematic representation of how electromagnetic wave can couple with metallic thin film via (a) Kretschman-Reather configuration. (b) Otto configuration.[21]

In both Kretschman and Otto configurations shown in Figure 4a and 4b the coupling condition for SPR is met only by p-polarized light, since the angle of p-polarized light controls the projection of the interfacial wavevector k_x. At the proper angle the optically driven k_x matches the intrinsic k_x of the SPP in the thin film. S-polarized light cannot couple to k_x of the

SPP in the thin film conductor. Under the coupling condition the incoming light energy of p-polarized light is absorbed by the SPP. Experimentally, this can be observed as a drop in the externally reflected light intensity, which is the essence of the SPR signal. The Kretschmann configuration is usually used to excite surface plasmons while the Otto configuration is typically used to excite bulk plasmons.

2. Materials for mid-infrared applications

Historically, SPPs have been investigated in noble metals: gold (Au) and silver (Ag). These noble metals have played the dominant role in SPR development because their plasma frequencies are in the visible region[27-29]. Despite the fact that the plasma frequencies of most metals are located in the deep ultraviolet[30-32], visible plasmons in Au and Ag are observed due to the d-orbital contraction in the late transition metals, which leads to relativistic effects that lower the energy of the d-band. [22] The net effect is that the Au and Ag plasmon resonance frequency becomes coincident with the onset of band-to-band transitions with energies in the visible range. However, this interband mixing also causes the plasmon bands of Au and Ag to have significant losses due to absorption in the visible and near-UV.[22, 33, 34] Although Au is known to be the more lossy material compared to Ag in the visible region of the spectrum, it has been more widely used because it is more inert and the plasma frequency is further to the red (8.89 eV[32]), which is more convenient for many experiments. It is evident from a study of the dielectric functions that Au and Ag both have significant mixing of band-to-band transitions into the SPP. By contrast, ITO does not have any such mixing.[35] As mentioned previously, the ITO band gap is ca. 3.2 eV, which is far higher in energy than the bulk plasma frequency, which corresponds to an energy of 1 eV. Consequently, the Drude free electron model is quite accurate as a description of ITO and indeed other CMOs that have been studied. These facts are well known, but it is less appreciated that because of the losses due to interband mixing neither Au nor Ag has a pure plasmon polariton, defined as the SPP of a free electron conductor.

Although it is theoretically possible to induce the SPP of Au and Ag in the IR frequency range, there are practical limitations.[36, 37] While SPR has been observed in Au thin films in the near-IR region, the Au loss function increases strongly as the frequency is lowered and there has

been no similar demonstration of SPR in the mid-IR.[38] The intraband loss is an inherent aspect of any conductor, which arises from the imaginary part of the Drude model. Any conductor is predicted by the theory to have an increase in loss below the plasma frequency.[39] Therefore, it is important to match the plasma frequency as closely as possible to the wavelength region of interest. Other metals have even higher plasma frequencies and are even less suited for SPR in the visible/IR than Au and Ag. These limitations led to a search for new materials supporting SPPs in the mid-IR. These are mainly semi-conductors, doped Si, GaAs, InP, GaN, as well as metal nitrides and oxides. Si and other (III-V) or (II-VI) semi-conductors have SPPs below the mid-IR while the metal nitrides have SPPs above the mid-IR.[40] Graphene is also an interesting candidate, but like traditional semi-conductors it has a sufficiently small concentration of free carriers to render it impractical for mid-IR applications. CMOs (ITO, Al:ZnO, Ga:ZnO, CdO:Dy, F:SnO_2, $SrRuO_2$ and many others) have shown superior properties when compared to metal nitrides.[39-41] Thus, CMOs have dominated the field of mid-and near-IR plasmonics. Of these, ITO has been the workhorse in most studies because of its wide availability due to its many commercial applications. A key point in this review is that the successes of ITO as a breadboard for laboratory study are overshadowed by limitations that make ITO a poor material for practical applications. The field has focused on the fact that CMOs consist of a range of different doped metal oxide materials that present possibilities for engineering of materials that have the desired wavelength range and quality factor for practical applications.

2.1 Engineering CMO optical properties in the infrared region

The infrared region of the electromagnetic spectrum carries vibrational information about chemical bonding and is widely used for detection of thermal contrast. There has been great interest in investigating the optical properties of CMOs for their potential applications in optoelectronic applications in the mid- and near-IR. Although there are only a handful of metal oxides that are good candidates for the applications, the number of possible new materials is nearly limitless when one considers the possible dopants, which are always an essential ingredient in the design of CMOs. Thus, a substantial research effort has been devoted to finding a robust material that can support SPP with low optical loss and tunability across the infrared region. Beyond SPR there has been a great deal of interest in CMOs as metamaterials based on the tuning of the ENZ in both thin films and nanostructures. Typical values of the ENZ mode are

shown in Figure 5 for a number of CMOs. The observed spectral location and bandwidth of the SPR and ENZ are correlated, which means that Figure 5 also permits the prediction of SPR to be observed at slightly lower energy than the ENZ energies shown. Therefore, our discussion of the material parameters applicable to the design of SPR spectra has obvious implications for the ENZ mode as well. We will focus on the material properties, doping and preparation of thin films of CMOs used for these applications and relate those to the free electron model in order to develop an understanding of the design aspects that have been used to push the optical properties into the mid-IR. CMOs are bracketed by metals to higher ENZ mode energies and traditional Si or GaAs semi-conductors to lower ENZ mode energies, each of which has a long history of plasma resonance phenomena. In the next two sections we discuss how these two different materials give us insight into the versatility of CMOs.

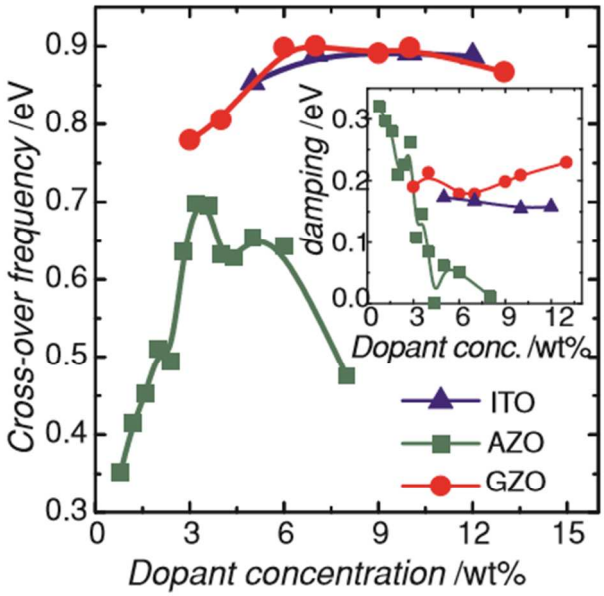

Figure 5. ENZ mode frequency of indium-tin-oxide (ITO), Ga:ZnO (GZO) and Al:ZnO (AZO) as a function of dopant concentration. Insert: Drude damping as a function of dopant concentration. Reprinted with permission from Ref ([40]). Copyright 2011 Optical Society of America.

2.2 Optical losses as a limitation to plasmonic applications in metals

Since the plasmons in CMO degenerate semi-conductor materials are much lower in energy than the band gap or any other band-to-band transitions, we have called these "pure plasmons".[35]

Figure 6 shows the contrast between the optical response of ITO and those of Au and Ag. Au has absorption in the visible and UV above the plasma frequency, which is clearly observable as the peaked feature in the red, imaginary part of the wave vector that is also associated with the loss in the material. Au has significant increase in absorption or loss above the plasma frequency due to interband transitions. Figure 6 also shows that Ag has a much smaller contribution from interband transitions, which explains why Ag has been the choice for high quality plasmonic material, despite its known disadvantage as a thin film material due to its high surface reactivity. ITO was the first material investigated for its potential as a near-IR or mid-IR SPR material.[6] The path to discovery of an infrared plasmonic material that possesses a high quality factor that rivals Au or Ag in the visible involved consideration of a series of CMOs starting with ITO and leading finally to the current highest quality factor observed in doped CdO.

The comparison of the dispersion curves in Figure 6 reveals a striking similarity between ITO and Ag.[35] The real response (blue) represents dispersion and plotted as ω vs. k to show the dispersion of the material. The imaginary wave vector response (red) represents absorption of light due to the ENZ. The peak of the absorption is coincident with the plasmon band gap. In theory this is the mid-point between the top of the SPP and the starting point of the BPP (see Figure 3). The dielectric curve of ITO was obtained from the Drude model based on the measured values of n and ε_∞, while Au and Ag were obtained from measured dielectric functions. As shown in the Figure 6, the dispersion curve of ITO has a relative width and shape that resembles the dispersion of Ag, although the wavenumber range for ITO is a factor of 4 lower than that of Ag. Ag has extinction to higher energy than the bulk plasma frequency, but ITO has essentially no extinction on the high energy side of the bulk plasma frequency below the bandgap (Figure 6A). Although Ag is considered the most suitable metal for plasmonic applications based on its spectral features, ITO has a "purer" plasmon than Ag. Unlike Ag or ITO, Au has a significant contribution from a d-to-p interband transition, which can be observed in nanoparticle absorption spectra. This additional absorption at or above plasma frequency shown in Figure 6B is not present in ITO and to a much smaller extent in Ag (Figure 6C).

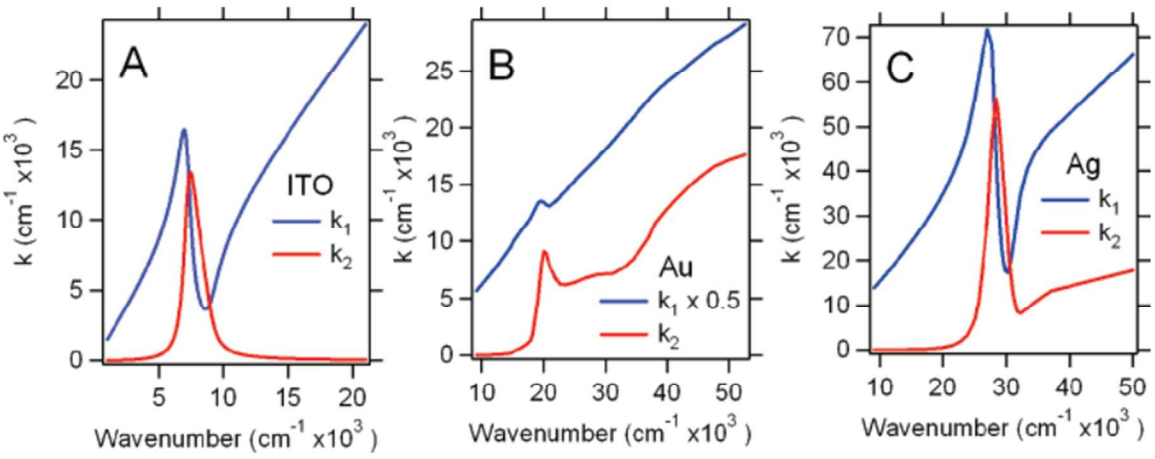

Figure 6. The real (blue) and imaginary (red) response of wave vectors for (A) indium tin oxide (ITO) (B) gold (Au) and (C) silver (Ag). Reprinted (adapted) with permission from ([35]). Copyright (2008) American Chemical Society

Although the noble metals are not tunable (i.e. in terms of their material properties), they can be prepared as arrays or nanoparticles (nanostructures) that provide a seemingly limitless tunability due to their shape.[42] The LSPR of Au and Ag depends on the aspect ratio and aggregation state of nanorods and nanoparticles.[43, 44] The creation of ordered arrays of gold on patterned surfaces has led to new ways to tune the LSPR of materials.[45] These aspects of the noble metals are currently being used as the pattern for similar experiments using CMOs.[46]

2.3 Far-IR SPR in indirect bandgap semi-conductors and graphene

The optical properties of doped silicon, which include its bulk plasma frequency, have been known for decades.[47-49] In addition, silicide materials have been studied more recently for plasmonic optical properties.[50, 51] The solid solubility, the upper limit of impurity concentration that can be absorbed by the material, does not permit a sufficiently high dopant concentration to reach the levels observed in many CMOs. Phosphorous has the highest solid solubility for silicon at 10^{21} cm^3. However, as the doping concentration approaches the solubility limit, the doping efficiency decreases, which presents an intrinsic limitation to applications based on these materials.[52] In the final analysis, the free carrier concentrations in doped Si are so low that none of silicon-based materials are suitable for mid-IR applications.

Germanium is more promising for SPR applications because it has a higher electron mobility than silicon[53-55]. Germanium has a smaller optical bandgap than silicon and is typically doped with gallium, aluminum and arsenic. Much like silicon, the solid solubility limit for dopants in Ge do not permit high doping levels. Arsenides[8, 56], Phosphides[57] and Nitrides[40, 58] have also been studied for infrared plasmonic applications. Although some of these materials have applications in the far-IR, none of these materials are ideal materials for optical application in the mid-IR region. The free carrier density of both doped Si and Ge limit the optical tuning range for the plasmons of both Si and Ge semi-conductor materials to the far IR.

Graphene has attracted attention as a 2-D material that can support SPR and also may have applications as a metamaterial.[59-62] Graphene can support surface plasmons in the mid-IR region, but only at low temperature (4.2K) because of high losses at room temperature. It is worth noting that the limited data available indicate that CMOs have a modest temperature dependence of both their band gaps and carrier densities.[63] Similarly heavily doped Ge, which has carrier densities in the same range as graphene shows a modest temperature dependence on carrier density.[54] Thus, the temperature dependence of SPR in graphene is an anomaly. As a practical matter graphene has SPR resonance at wavelengths > 6.5 μm under ambient conditions, which makes it most useful in the far-IR, the same region accessible to the plasmons of traditional doped semi-conductors.[64]

2.4 Transparent Conducting Oxides as mid-IR and near-IR SPR Materials

In 2002, Franzen and Brewer hypothesized that pure plasmons can be observed in CMOs based on the correlation of surface resistance a decrease of reflectivity in ITO in the near-IR region.[4, 65] Based on the understanding of the semi-conductor SPP, which was known at the time, it was predicted that ITO would have the potential for SPR applications in sensing in the mid- and near-IR analogous to Au in the visible. The prediction based on the reflectivity correlation was observed in the detection of SPR in ITO in 2006 using a $\theta - 2\theta$ stage attached to a Fourier transform infrared (FTIR) spectrometer.[66, 67] The optical response of ITO films was studied as a function of thickness from 30 nm to 300 nm.[11] Subsequently, the effect of thin film preparation on the optical properties was quantified based on the Drude model.[68] The use of hybrid Au:ITO plasmonic thin films permitted a separation of the SPP and ENZ based on polarization.[10] The SPP can be excited by electromagnetic (EM) radiation aligned parallel to the interface of the thin

film and the ENZ can be excited only by EM radiation polarized perpendicular to the film surface.[10] While these studies demonstrated the utility of ITO as a material for theoretical study of SPR in the near-IR the understanding derived from these studies led to the conclusion that the quality factor of the SPR signal was approximately 5 times lower than that of Au because of the low mobility of ITO (ca. 30 cm^2/Vs). Further experimental studies failed to find a feasible preparation of a thin film of ITO with significantly higher mobility. Thus, these initial studies revealed the need to investigate other CMOs focusing on maximizing the carrier mobility.

Attention was then focused on zinc oxides (ZnO). These metal oxides are also transparent to visible light because of their large bandgap. Like ITO, doped-ZnOs are referred to as transparent conducting oxides (TCOs). ZnO be doped degenerately to achieve conducting thin films that possess metal like properties in the mid-IR and near-IR range. Conducting films, aluminum-doped ZnO (AZO) [13, 69-71], gallium-doped ZnO (GZO)[12, 39, 69] were thoroughly investigated as potential candidates for NIR applications. AZO thin films have lower losses with high doping, but GZO and ITO have higher carrier concentrations.[4, 72] Figure 3 depicts the carrier concentration of the three materials as a function of doping concentration. While these materials are tunable, easy to prepare and cheaper than ITO, they have the same disadvantage in that the mobilities are quite low. None of the doped ZnO films studied to date has a quality factor that is an improvement over ITO. The systematic study of ITO using the Drude model as a guide for design led to an understanding of the role played by the mobility in the SPR of CMOs. Ultimately, this process of measuring the optical response of various thin films pointed towards to a new class of doped CdOs, which are the most promising materials to date for mid-IR SPR applications.

2.5 Indium tin oxide as a testbed material for near-infrared plasmonic applications

ITO thin films are widely used in heat shielding materials[73-75] and electrochemical sensors[76, 77] due to its optical properties being sensitive to small variations in their preparation and annealing procedures. Hence, ITO is widely used as an infrared reflector and as transparent electrode in the visible region.[78-81] The observation that the ITO reflectance decreases in the near-IR region proportional to the conductance of the respective thin film lead to the hypothesis that ITO has potential as a plasmonic material in mid-IR region.[4, 82] Using the Drude model, the plasma frequency of ITO was predicted to occur in the near-IR region. Due to its band structure,

ITO is an excellent material for direct observation of the optical properties within the conducting, resonance and insulating regimes. The effects of the free electron theory have been tested in ITO without interference from band-to-band transitions. The extinction in Ag and even more so, those in Au (Figure 6B and 6C) arise from strong interband transitions, which deviate significantly from the free electron model. While the Drude model has great predictive power for ITO and other CMOs it has little utility in studies of the noble metals.

In the conducting regime, the electrons follow the incident electric field leading to complete reflection in the absence of absorption losses ($\omega < \omega_p/\sqrt{\varepsilon_\infty} = \omega_{bp}$). ω_{bp} is the frequency of the bulk plasmon and ε_∞ is the high frequency dielectric constant. In the resonant regime, $\omega = \omega_{bp}$, one can excite the ENZ mode. When this was initially observed in very thin films of ITO, we called this observation a capacitive plasmon resonance (CPR) to indicate that the field excitation is perpendicular to the surface[10]. This perpendicularly polarized resonance, which is most commonly known today as the ENZ, has been known both from Abeles early work on conducting films [83] and the analogous effect in insulating films, known as the Berreman mode.[84, 85] The ENZ mode is only observed in thin films that are thinner than the skin depth of the conductor. The ENZ mode has never been observed in Au or Ag because their skin depths are so shallow (< 5 nm) and surface free energy is so high that it is essentially impossible to deposit a film that is thinner than the skin depth. However, ITO has a skin depth of ~120 nm for films that have ENZ modes in the near-IR. Mid-IR SPR materials such as CdO have skin depths > 200 nm due to their lower carrier density. The ENZ mode is related the localized surface plasmon resonance (LSPR) in a nanoparticle, although there will be a geometrical effect that shifts the location of the resonance. Since the LSPR depends on particle size and shape the thin film value of the analogous resonance is not precisely in the same region as the LSPR. One might think of the thin film as a nanoparticle stretched out so that it forms a film. For example, in ITO the ENZ mode (CPR) is observed at ~9,000 cm^{-1} [10] in a 30 nm thick film. The ENZ mode in a hexagonal geometric array of ITO triangular patterns with a thickness of 20 nm is observed at 6,200 cm^{-1}.[46] The LSPR of ITO observed in nanoparticles at the same doping of 10% Sn is 6,200 cm^{-1}.[86] While it is difficult to know the exact carrier density in the nanoparticle the comparison underscores a basic similarity between the wave number range of the ENZ and LSPR. Numerous experiments on a variety of different CMOs show that the frequency of the ENZ mode and SPP are correlated, and both are controlled by altering the charge carrier density.

Below the bulk plasma frequency $\omega < \omega_{bp}$, light can couple into the material if it propagates through an optically dense medium that permits total internal reflection at the boundary. SPR can be observed by coupling light into a conducting layer such that there is a propagating wave along the insulator-conductor interfaces on both sides of a conducting thin film and an evanescent wave that penetrates into the conductor as shown in Figure 4. When light propagates through vacuum or air, it is reflected for $\omega < \omega_{bp}$. When $\omega > \omega_{bp}$, ITO behaves optically as an insulator and it is transparent in this regime. This observation underlines how different the material interacts with EM waves dependent on their energy relative to the plasma frequency. While these statements are true for any plasmonic material, they are much easier to visualize in the CMOs. Despite its limitations for practical applications, ITO is still a useful material for demonstrating the predictive utility of the free electron theory for engineering CMOs as plasmonic materials.

2.6 Experimental considerations behind the first observation of SPR in ITO

The detection of SPR in a conducting metal oxide was first achieved using a FT-SPR attachment for a FTIR spectrometer constructed by GWC Inc. (Madison, WI) in 2006.[36, 37] ITO has one of the highest charge carrier densities of any CMO, thus, it is well suited for measurements in the near-IR range (5000 – 9000 cm^{-1}). The dependence of the SPR signal on the thickness of the conducting film can be explained by referring to three thickness regimes.[11] First, very thin ITO films of less than ~120 nm cannot support SPPs when used in Kretschmann configuration because the phase shift in the evanescent field propagating through the cannot match that of the incident radiation at any angle.

In order for incident light to couple into the SPP (see Figure 4) the conduction electrons must oscillate in the vicinity of the conducting-insulator interface and result in an evanescent field that decays exponentially, perpendicular to the interface, into the metal as well as the dielectric. This decay has a limited penetration depth and known as skin depth. The skin depth is related to the decay of the magnitude of the electric vector (E) [22] in ITO by

$$E = E_0 \exp(-t/\delta) \tag{2.1}$$

$$\delta = \frac{c}{(2\pi\sigma\mu\omega)^{1/2}} \tag{2.2}$$

where t is the thickness of ITO, E_0 is the original magnitude of the electric vector, c is the speed of light and σ is the conductivity.

A film that is thinner than the skin depth of the conductor does not permit an electric field oscillation along the conductor-insulator interface. This condition is present in panel 7A and 7B where the thicknesses are 30 nm and 55nm, respectively. There is no SPR signal and the observed extinction is the ENZ mode in those panels. There is a transition between two regimes shown in Figure 7C and 7D where multiple optical features are present. The optimal thickness for ITO films is observed to be between 120-200 nm, which is shown in Figure 7E, 7F and 7G. In this thickness range the phase shift induced by the loss tangent of the metal can match incident radiation in the near-IR frequency range. In this thickness regime, ITO film can support SPP and an angle-dependent SPR signal can be observed. The optimal thickness for the most common ITO thin film preparation (10% Sn annealed in forming gas) is approximately 160 nm. In the third regime when the film thickness increases beyond the optimal value the SPR signal decreases in magnitude as shown in Figure 7H. As the thickness surpasses 200 nm the loss tangent increases to the point where it is no longer possible to achieve a matching condition. Viewed from another point of view the SPP is reduced proportional to the reduction in the evanescent field at the second conductor-insulator interface. The SPR signal eventually vanishes as is evidence in Figure 7I.

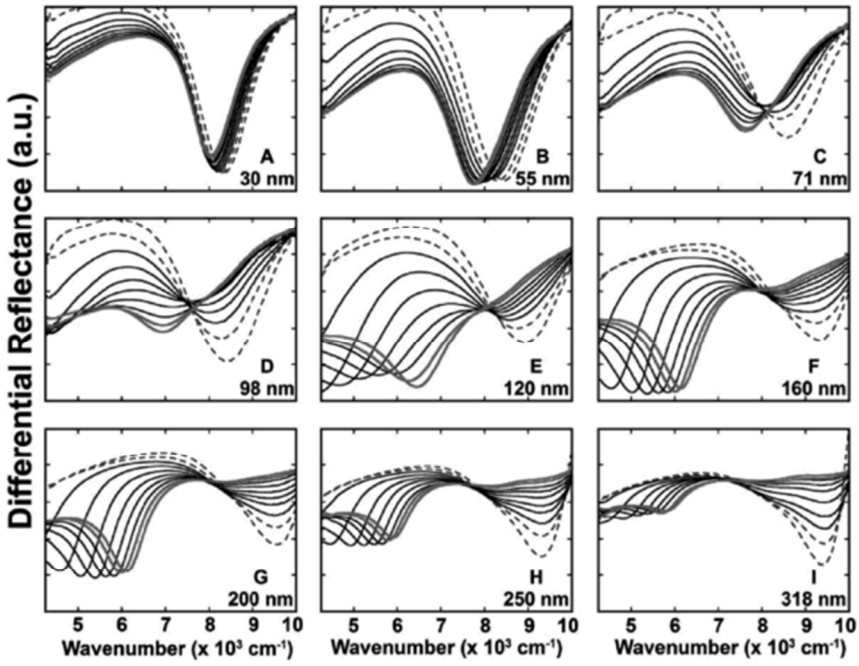

Figure 7. SPR spectra R_p/R_s obtained for ITO film thicknesses d from 30 (panel A) to 318 (panel I). Each line represents an angle increment of 0.83°. Used with permission from Ref ([87]).

The SPP band is tunable with carrier concentration as depicted in Figure 8. The plasma frequency shifted to lower energy as *n* decreases as depicted in eq (1.4). Although ITO was a testbed material for infrared SPR, it has one major drawback. ITO has a low carrier mobility (30 cm^2/Vs), which leads to a broad SPR response.[11] The width of the SPP band increases as the mobility decreases as shown in Figure 9. This realization provides a systematic approach to search for high mobility conducting metal oxides that can overcome this problem in the near and mid-infrared region. The push to the mid-IR region is a pragmatic consideration since most conducting metal oxides have charge carrier densities lower than ITO, which naturally places them in the mid-IR region, which is also the region where molecular vibrations are observed by FTIR spectroscopy.

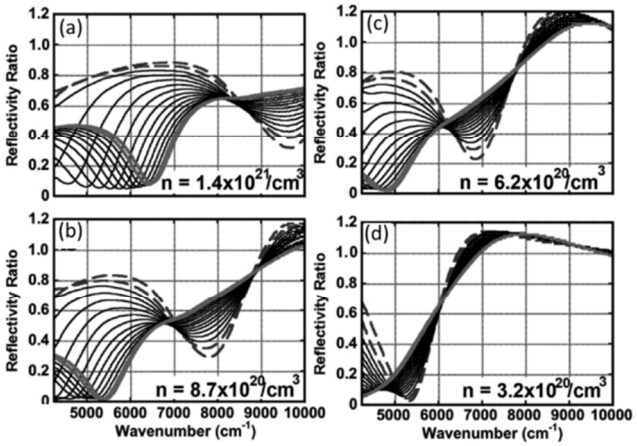

Figure 8. The experimental and theoretical data for the carrier concentration series. The corresponding charge carrier densities are given in each panel. Used with permission from Ref ([87]).

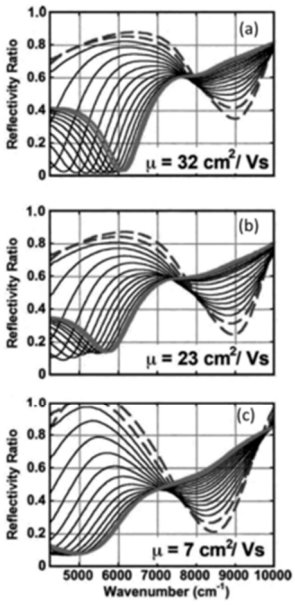

Figure 9. The experimental data of mobility series, where the sputtering pressure of the target gas is 9 mTorr for (a), 12 mTorr for (b), and 15 mTorr for (c). The corresponding mobilities are given in each panel. Used with permission from Ref ([87]).

ITO has been widely used in a variety of mid-IR plasmonic applications. The tuning of plasmons in ITO is possible using carrier accumulation to modify the carrier density, which in turn affects ω_p and the observed SPR reflectance minimum. [88] A large non-linear optical signal was observed near the ENZ mode of ITO using ultrafast spectroscopy. [41] Switching of the ENZ using ITO in a waveguide sandwiched between two Au electrodes has also been demonstrated. Each of these applications shows how externally applied electric and optical field fields can be used for photonic switching in CMO-based plasmonic materials. ITO is still the most useful CMO for general demonstration of the possible photonic applications. But, materials in the mid-IR with higher quality factors may ultimately provide the most interesting for end user applications that involve heat measurement and capture, IR detectors, molecular sensing, nanoscale spectroscopy, and optical circuits.

2.7 The Search for Appropriate Conducting Metal Oxides for mid-IR Applications

Once SPR in the near-IR region was established by the experimental observations in ITO, the quest for new CMO materials with high mobility began in earnest. Most CMOs have carrier densities lower than those of ITO so that the majority will have SPR in the mid-IR.

Perovskite oxides[89, 90] such as $SrTiO_3$, $SrSnNO_3$, Cd_3TeO_6 and $SrGeO_3$ were studied as potential candidates for infrared SPR. Though some of these materials are found to be useful in other areas such as solar cells and superlenses[91, 92], it was realized that none of these materials can match the maximum supported free carrier density of doped ZnO and ITO. Heteroepitaxial thin films of ZnO were also explored as a potential host for infrared plasmonics.[14] Spectroscopic detection of SPR was demonstrated for ZnO in the mid-IR region between 2000 and 3000 cm^{-1}. Though ZnO can support mid-IR plasmonics, the observed SPR was broad and lossy as shown in Figure 10. Figure 10 shows experimental data in the 2-D map format (angle vs. cm^{-1}). Figure 10b shows a doped ZnO film with optical thickness for observation of SPR. The black region, which corresponds to the extinction due to the SPR, is very broad. This is a consequence of the low quality factor, which in turn is due to the low charge carrier mobility at the carrier concentration ($4 \times 10^{19} - 8 \times 10^{19}$ cm^{-3}) needed to sustain mid-IR SPR.

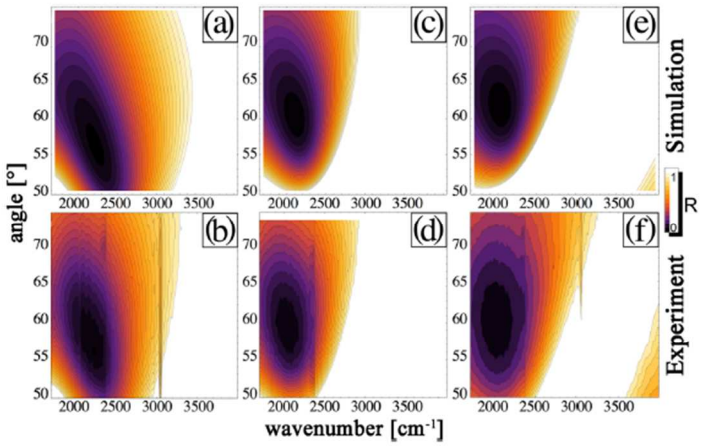

Figure 10. Simulation and experimental reflectivity data comparison for Zinc oxide (ZnO) with different film thicknesses. (a,b) 400 nm (c,d) 600 nm (e,f) 800 nm. (a,c, and e) are simulated data. Reprinted from [14], with the permission of AIP Publishing.

A rational materials search based on the collective experience of the preceding IR plasmonic materials permitted Sachet et al, to propose and demonstrate cadmium oxide doped with dysprosium (CdO:Dy) as a gateway material for development of high-quality-factor tunable SPR in the mid-IR region in 2015.[9] Subsequently, the materials set was expanded and a family of

doped CdO:M (M = Dy, Y, F etc.) exhibits sufficiently high mobility to support SPR at mid-IR energies with low optical losses.

2.8 CdO:Dy: A Gateway Material for Mid-IR SPR

In 1969, the material properties of an intrinsic single crystalline CdO were reported by Koffeyberg.[93] According to the data in Ref. 89, single crystal CdO exhibits both mobilities and carrier densities needed to support high quality mid-IR SPR. Simulations of the predicted optical response for CdO in the mid-IR were conducted using the Fresnel equations combined with the free electron model to approximate the CMO dielectric function. Subsequently, a thin film growth method was developed using dysprosium (Dy) as a dopant. CdO doped with Dy (CdO:Dy) thin film was observed to have low loss in the mid-IR due to its unusually high mobility[9] at carrier concentrations $>10^{19}$ cm^{-3}. The observed electron mobility was achieved through defect equilibrium engineering of the CdO native and extrinsic crystallographic defects. Although there are numerous candidate dopants that one can consider for CdO, Dy was the first dopant used to successfully demonstrate this effect.

CdO is an intrinsic n-type semiconductor where free electrons originate from doubly ionized O-vacancies (equation 3.12). By doping CdO with Dy, Dy populates the Cd sublattice with 3^+ charge and acts as extrinsic donor (equation 3.13). The defect equilibrium system of intrinsic and extrinsic defect reactions is given as:

$$\mathrm{Cd}_{\mathrm{Cd}}^{\mathrm{x}} + \mathrm{O}_{\mathrm{o}}^{\mathrm{x}} \Leftrightarrow \mathrm{Cd}_{\mathrm{Cd}}^{\mathrm{x}} + \mathrm{V}_{\mathrm{o}}^{\bullet\bullet} + 2e + \frac{1}{2}\mathrm{O}_2 \tag{2.3}$$

$$\mathrm{Dy}_2\mathrm{O}_3 \underset{\Longrightarrow}{CdO} 2\mathrm{Dy}_{\mathrm{Cd}}^{\bullet} + 2\mathrm{O}_{\mathrm{o}}^{\mathrm{x}} + 2e + \frac{1}{2}\mathrm{O}_2 \tag{2.4}$$

Although dysprosium on a Cd-site and an oxygen vacancy are both electron donors, Dy substitution gives rise to a smaller lattice perturbation than an oxygen vacancy. The lattice disruption of Dy doping is small because Cd and Dy have similar ionic radii ($\mathrm{r}_{\mathrm{Cd}}^{2+} = 0.95\ \mathrm{nm}, \mathrm{r}_{\mathrm{Dy}}^{3+} = 0.92\ \mathrm{nm}$). [94] The singly charged n-type donor, $\mathrm{Dy}_{\mathrm{Cd}}^{\bullet}$ in eqn. 2.4, increases at the expense of the doubly charged n-type vacancy, $\mathrm{V}_{\mathrm{o}}^{\bullet\bullet}$ in eqn. 2.3 and the net effect of this replacement is a decrease in lattice strain and a concomitant increase in mobility in parallel with the increase in charge carrier density over a range of dopant concentration. Because impurity scattering scales with Z^2, there is less net scattering for *2n* donors of charge *e* than *n* donors of

charge 2*e* at the same carrier density. These phenomena lead to the observed increase in mobility up to a threshold charge carrier density above which the defect equilibrium is weighted towards $Dy_{Cd}^{\bullet}$ and the scattering from Dy begins to dominate. These competing effects define the useful range of free carrier concentration within CdO that gives rise to a tunable, narrow bandwidth plasma resonance in the mid-IR region. The transport properties of CdO:Dy at room temperature are presented in Figure 11. The conductivity and carrier concentration are both observed to increase as Dy doping concentration increases spanning the range of 5 $x10^{19}$ – 1 $x10^{21}$ cm^{-3}. Mobility follows the same trend until it reaches its maximum mobility value of 500 $cm^2V^{-1}s^{-1}$ at 5 x 10^{19} cm^{-3}. Beyond this Dy concentration, carrier mobility decreases until the limit of 5 x 10^{21} cm^{-3}. This unique combination of high carrier density and mobility of CdO:Dy makes it an ideal plasmonic host at mid-IR frequencies.

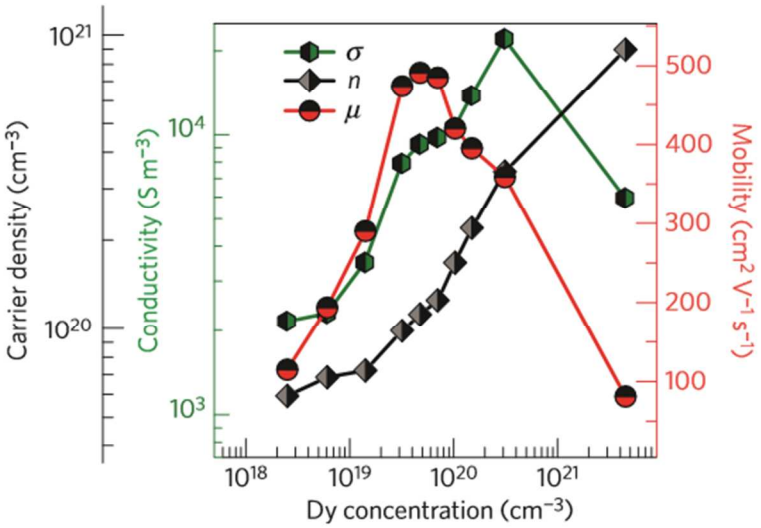

Figure 11. Transport properties of CdO:Dy carrier concentration (n), carrier mobility (μ) and conductivity (σ) as a function of Dy concentration. Reprinted by permission from Macmillan Publishers Ltd: Ref [9], copyright (2015)

To demonstrate the optical properties of CdO experimentally, a series of samples was investigated spectroscopically. In Figure 12, experimental and simulated data are presented for two CdO:Dy films with two sets of mobility es and carrier concentrations. Simulations are set up

to optimize the ideal condition for the substrate by incorporating all optical components of the experiment. The SPR data were recorded in the Kretschmann configuration using a Woollam® IR-Variable Angle Spectroscopic Ellipsometer (VASE). As mentioned for ITO in section 2.4, the phase shift has to be accounted for experimentally by varying the thickness of the CdO thin films. Extremely smooth CdO:Dy substrates presented in Figure 12 were grown using an oxide molecular beam epitaxy (MBE) environment. Figure 12b shows the experimentally determined SPR dispersion curve as the black curve. The black color indicates extinction due to plasmonic resonances. The relatively narrow feature of this curve is an indication of a high quality factor, which is attributable to the high mobility of 478 cm^2/Vs. The reader should compare this 2-D plot to that of Al:ZnO in Figure 10b. The SPR dispersion feature in the 2-D of Al:ZnO should be curved in the same way as the one is in Figure 12b. However, the feature is so broad in Figure 10b that is not possible to discern its shape. Figure 12d shows a thin film that has a significantly high free carrier density (3.3 x 10^{20} cm^3 in Figure 12d compared to 1.3 x 10^{20} cm^3 in Figure 12b). As a consequence, the ENZ is shifted 3,500 cm^{-1} in Figure 12b to a value greater than 3,800 cm^{-1} (i.e. it is no longer visible on the plot of Figure 12d because it is shifted to an energy to the right of the plot limit).

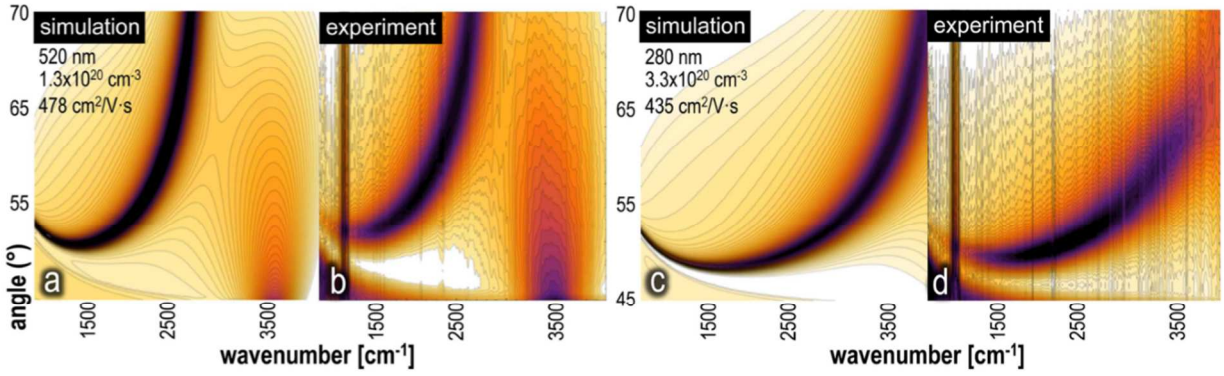

Figure 12. Simulated reflectivity data and experimental data of CdO:Dy with thickness of 520 and 280 nm by varying mobility and carrier density. Reprinted by permission from Macmillan Publishers Ltd: Ref [9], copyright (2015)

2.9 Further advances in CdO:M doping (M = Dy, Y, F) and in thin film preparation

Highly accurate doping using MBE was the key to investigate the structure property relations in CdO:Dy. However, the limited throughput and high cost of MBE present a barrier to larger scale application of this material. Recently, thin films have been prepared using several other dopants by RF-assisted reactive High-Power Impulse Magnetron Sputtering (or HiPIMS). [95, 96] These dopants include yttrium and fluorine, among several others. Notably, CdO:Y grown via HiPIMS demonstrates mobility in excess of 400 $cm^2V^{-1}s^{-1}$ with a carrier density of ~10^{20} cm^{-3}. For films grown on sapphire, these results are superior to those achieved using MBE. Furthermore, it has been demonstrated that the carrier density can be reproducibly tuned between low 10^{19} and mid 10^{20} carrier concentrations by controlling the magnetron power and the cathode to substrate distance for the dopant source. With dopants such as dysprosium, yttrium and fluorine in conjunction with multiple deposition methods, one can engineer doped CdO with tailored properties suitable for a variety of applications, permitting doped CdO to become a model material for high quality mid-IR plasmonic applications. [95, 96]

3. IR Localized Surface Plasmon Resonance (LSPR) in doped CMO nanocrystals

The localized surface plasmon resonance (LSPR) of nanocrystals in the mid-and near-IR region is another phenomenon that has recently received great interest. While SPR is related to the fields generated at the conductor-insulator interface of a thin film, in LSPR, the dimensions of the nanostructure are small relative to both the skin depth of a conducting film and to the wavelength of the incident radiation, λ. For spherical particles the radius, $R << \lambda$. The scattering of light from spherical Au and Ag particles that meet this condition are well described in terms of the spherical harmonics as described in Mie theory.[97] We can think of the extinction by particles as related to the absorption by the ENZ mode. This can be seen in ITO where both LSPR and the ENZ have been measured experimentally.[10, 11,46,86] However, the frequency and line shape of LSPR is dependent on particle shape as well, so the correspondence between the ENZ and LSPR is not expected to be exact. The ENZ is polarized perpendicularly to a thin film surface. This experimentally demonstrable fact led to the alternate designation CPR for this extinction.[11] The name ENZ focuses attention of the remarkable fact that all of the absorption occurs between the two interfaces of the conducting thin film. There is an amplification of the electric field due to the trapping of energy in the small space of a thin film that is less than a few hundred nanometers in thickness. On the other hand, the CPR designation focuses attention on

the fact that the polarization of this trapped field is perpendicular to the surface of the film. The ENZ/CPR is a "bulk" effect rather than a surface effect. The meaning of the word bulk must be adapted to conditions where the film is so thin that it has properties relevant to both surface and bulk. The thin film observations are connected to what is called LSPR because by increasing aspect ratio, one can observe two extinctions, parallel and perpendicular to the axis of an ellipsoid. A thin film is an extreme limit in which there is an ENZ (CPR) extinction perpendicular to the film of defined thickness and SPR parallel to the film surface, which is essentially infinite on the length scale of the incident radiation.

The experience with Au and Ag leads to an understanding of aspect ratio and particle size as two factors that can modulate the extinction of particles over a wide range. Using geometric design, LSPR bands of Ag nanoplates and nanorods have been extended into the mid-IR region.[102, 103] However, while Ag and Au nanoparticles show geometric tuning, CMOs can also be tuned using doping. i.e. a material property. Thus far, the growth of CMO particles has been confined to more nearly spherical shapes so the experimental possibilities to test these relationships are still a rich area for investigation. Metal oxides are readily structured into nanocrystals. New syntheses[98-100] are emerging and there are clearly many possibilities for the use of LSPR in CMOs.[101]

The tendency of Ag and Au to aggregate is much larger than for CMOs. Therefore, the colloidal instability of Ag and Au is much larger because the Hamaker constant of Ag and Au is about 5 times later than for typical oxides. Moreover, since the bulk plasma frequencies of CMOs are much lower than metals such as Au and Ag, the frequencies of doped CMO nanocrystals can be easily tuned to the mid-IR, which is difficult to achieve for the noble metals even with the most ambitious geometric tuning. It should be born in mind that although the concept of SPR and LSPR are similar, it is actually the ENZ that has the greatest similarity to the LSPR. Like the ENZ, the LSPR is an extinction that does not involve angle-dependent coupling of the incident light. One could envision a very thin film as the limit of a high-aspect ratio nanostructure stretched to the limit of infinity in two dimensions. It is important to note that this hypothesis is substantiated by the fact that the ENZ observed in ITO[5, 6,10] observed in very thin films predicted the frequency of ITO nanoparticles with similar Sn doping.[86]

As in the field of thin films discussed above, ITO has been the testbed material used to push LSPR into the IR region in nanoparticles or nanocrystals.[15-17] The plasma frequency of ITO can be tuned across near-infrared (NIR) region by controlling the doping concentration of Sn. [86] It was also demonstrated that by using solution-phase chemical synthesis, LSPR of colloidal ITO NCs can be tuned from 1618 nm to >2200nm.[86] The structure of ITO nanoparticles also affects the strength of the IR absorption. Wang et al reported that bbc-ITO has a strong NIR absorption at 2000 nm whereas rh-ITO nanoparticles exhibits no IR absorption[104]. It was also observed that when In_2O_3 is co-doped with F and Sn, the cubic nanocrystals exhibit plasmon absorption in mid-IR range and it is observed to be coupled to C-H bond of surface-bound oleate ligands as shown in Figure 13.[105]

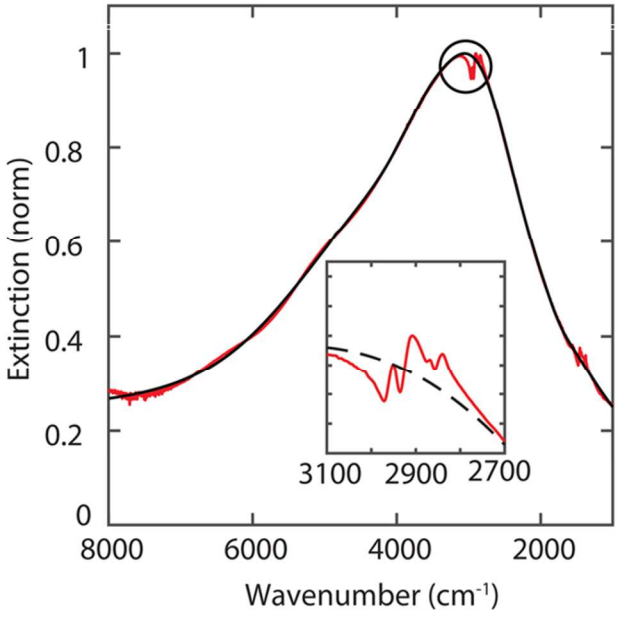

Figure 13: Extinction spectrum of 20 nm oleate ligands capped cubic nanocrystals, inset shows Fano resonance coupling signature. Reprinted by permission from ACS: Ref [97] http://pubs.acs.org/doi/abs/10.1021/acs.nanolett.7b00404, further permissions related to the material excerpted should be directed to the ACS.

ZnO nanoparticles have also been investigated for LSPR in the IR region. ZnO is inexpensive and provides the potential to explore size-dependent properties. Al, Ga and In are the most common dopants used in doped-ZnO films or particles. Indium doped ZnO (In:ZnO) gives high transparency in visible region and high IR absorption while having the highest dopant

efficiency over Ga and Al.[16] However, Bounsanti et al[106] demonstrated that it is possible to tune plasmonic absorption across mid-IR region by varying the dopant concentration of colloidal aluminum in ZnO nanocrystals. When Al concentration is varied from 1.4 - 7.3% in AZO nanocrystals, plasmon absorption can be tuned across mid-IR region.[106]

CdO has also been explored as a potential LSPR material in IR region. It was reported that CdO could be used to prepare the highest conductivities and carrier mobilities out of any TCOs when doping it with Sn. [107] CdO doped with Indium (ICO) NCs has been successfully synthesized with different shapes and shape-dependent optical responses have been demonstrated. [108] It is also reported that by using discrete dipole approximation (DDA), the dependence of field enhancement on size, shape and doping level concentration can be calculated. [109] The field of the LSPR has the potential to enable surface chemistry and can be probed using surface-enhanced Raman Spectroscopy (SERS), plasma enhanced fluorescence and other surface sensitive spectroscopies. The field of LSPR has progressed towards the near-IR and mid-IR in parallel with the SPR of thin films. The understanding of the relationship of the ENZ to the LSPR in these materials provides a predictive tool for the development of tunable mid-IR plasmonic particles.

4. Substrate Stability for Mid-IR Applications

Most applications of CMOs involve exposure to both air and water at moderate temperatures. Any layer that is water soluble will thus have limited applications. The water solubility of the various CMOs can be estimated using the Pourbaix diagram for the respective material.[110, 111] ITO is stable for pH > 3, but in solutions of pH < 3 ITO thin films rapidly dissolve. Consequently, under moderately strong acidic conditions ITO can be removed from a surface in minutes. ZnO films are more sensitive to water than ITO and begin to dissolve at pH 5. Finally, CdO is quite soluble in water even at pH 7, which limits the applications of CdO in aqueous media. To overcome this intrinsic disadvantage, CdO layers can be protected using atomic layer deposition (ALD) of SiO_2 or Al_2O_3. Recognizing this disadvantage points towards potential directions for future materials research where the stability in aqueous media needs to be optimized as well as the optical properties.

5. Conclusion: The future of SPR in the mid-infrared region

Due to its high carrier density and high mobility doped CdO:M (M =Dy, Y, F etc.) has a sharp plasmonic band in the mid-IR that competes favorably with the SPP band observed for Au and Ag in UV-Vis SPR. Though CdO:M proved to be an ideal plasmonic material for the mid-IR from an optical perspective, there are disadvantages to CdO as a thin film material. First, Cd and CdO are toxic adding constraints to processing and handling. Second, CdO dissolves readily in water and dilute acids, thus presents challenges for applications in aqueous environments. The future of the science and technology of mid-IR infrared plasmonic resonance lies in continuing the search for other CMOs with high mobility and carrier density that can replace CdO:M. It is possible that the mobilities of these new plasmonic materials may not quite match those of the CdO:M family, but there is a real prospect that a material can be found with a mobility in a useful range that is less toxic than CdO and stable in aqueous solution. The theory and ideas used in developing CdO:M can be implemented, and the process can serve as a road map to finding new plasmonic materials when exploring promising candidate materials such as GaN, ScN, $BaSNO_3$ and In_2O_3.

Applications of mid-IR SPR have already begun to emerge as doped CdO serves as a prototype for development of related materials that can solve specific technological problems. It has been reported that strong light-matter coupling of molecular transitions to plasmons is possible and has been observed in the visible region.[112, 113] This strong coupling is also possible in IR SPR and it is one of the research areas that the authors are currently exploring using doped CdO. Ideas of incorporating SPP as light capturing devices in various solar cells were also published in several papers,[104, 114, 115] but many CMOs explored were not as useful since the materials used in the experiments can only absorb light in wavelengths shorter than mid infrared regions, which is far from the peak of the solar spectrum. However, absorption for other applications such as filters and detection of IR light have been contemplated.

In addition to the CMOs discussed in this review, IR SPR propagation has also been observed in hybrid structures such as metal-insulator-metal (MIM) or insulator-metal-insulator (IMI) waveguides, where light is confined in the insulator between the metals.[116] Plasmonic waveguide has been an important application in on-chip optical data transfer in computer processing since it can confine light in dimensions smaller than its wavelength. Several new methods in confining light using plasmonic waveguides in telecommunication wavelength at

near infrared region have been reported using hybrid structures.[117, 118] Plasmonic waveguides also have application in the development of metal oxide semiconductor field effect transistors (MOSFETs) in the IR region.[119, 120] These transistors are widely used in switching electronic devices and amplifying signals. Plasmonic structures offer the possibility of miniaturization due to confinement of light to subwavelength dimensions. Therefore, the new materials reported in the mid-IR region may be used to improve the performance of plasmonic waveguide devices.

The field of infrared plasmonic applications has grown from a theoretical prediction to an established field in about a decade. The validity of predictions based on the Fresnel equations combined the effect of experimental material properties on the free electron model indicates a promising future as we search for new materials that can support tunable infrared SPP and ENZ modes with interesting applications. Initially the field was advanced by using ITO as a testbed for infrared plasmonics. Vital information was obtained that defined the characteristics of an ideal plasmonic thin film material. This understanding resulted in a rational search to discover a novel material. Starting from previously reported properties of CdO it has been possible to refine a growth method for doped cadmium oxides (CdO:M) that gave rise to a low-loss thin film conductor with high mobility and high carrier concentration.

Acknowledgement

This work was supported by NSF grant CHE-1507947.

References

1. F. Abeles, *J. Opt. Soc. Am.*, 1957, **47**, 473-482.
2. S. H. Brewer and S. Franzen, *Journal of Physical Chemistry B*, 2002, **106**, 12986-12992.
3. S. H. Brewer and S. Franzen, *J. Alloys Comp.*, 2002, **343**, 244-244.
4. S. H. Brewer and S. Franzen, *Chem. Phys.*, 2004, **300**, 285-293.
5. G. V. Naik and A. Boltasseva, *Phys Stat Sol-Rapid Res Lett*, 2010, **4**, 295-297.
6. C. Rhodes, S. Franzen, J.-P. Maria, M. Losego, D. N. Leonard, B. Laughlin, G. Duscher and S. Weibel, *Journal of Applied Physics*, 2006, **100**, 054905.
7. V. W. Brar, M. S. Jang, M. Sherrott, J. J. Lopez and H. A. Atwater, *Nano Lett*, 2013, **13**, 2541-2547.
8. S. Law, L. Yu and D. Wasserman, *J. Vac. Sci. Tech. B, Nanotech. Microelec.: Mater., Proc., Meas. Phen.*, 2013, **31**, 03C121.
9. E. Sachet, C. T. Shelton, J. S. Harris, B. E. Gaddy, D. L. Irving, S. Curtarolo, B. F. Donovan, P. E. Hopkins, P. A. Sharma, A. L. Sharma, J. Ihlefeld, S. Franzen and J. P. Maria, *Nat Mater*, 2015, **14**, 414-420.
10. S. Franzen, C. Rhodes, M. Cerruti, R. W. Gerber, M. Losego, J. P. Maria and D. E. Aspnes, *Opt Lett*, 2009, **34**, 2867-2869.
11. C. Rhodes, M. Cerruti, A. Efremenko, M. Losego, D. E. Aspnes, J. P. Maria and S. Franzen, *J Appl Phys*, 2008, **103**, 093108.
12. J. Kim, G. V. Naik, A. V. Gavrilenko, K. Dondapati, V. I. Gavrilenko, S. M. Prokes, O. J. Glembocki, V. M. Shalaev and A. Boltasseva, *Phys Rev X*, 2013, **3**.
13. T. Minami, H. Nanto and S. Takata, *Jap J Appl Phys 2-Lett*, 1985, **24**, L605-L607.
14. E. Sachet, M. D. Losego, J. Guske, S. Franzen and J. P. Maria, *Appl Phys Lett*, 2013, **102**.
15. G. Garcia, R. Buonsanti, E. L. Runnerstrom, R. J. Mendelsberg, A. Llordes, A. Anders, T. J. Richardson and D. J. Milliron, *Nano Lett*, 2011, **11**, 4415-4420.
16. E. Gaspera, A. Chesman, J. Embden and J. Jasieniak, *ACS Nano*, 2014, **8**, 9154-9163.
17. S. D. Lounis, E. L. Runnerstrom, A. Bergerud, D. Nordlund and D. J. Milliron, *J Am Chem Soc*, 2014, **136**, 7110-7116.
18. A. Alù, M. G. Silveirinha, A. Salandrino and N. Engheta, *Phys Rev B*, 2007, **75**.
19. S. Enoch, G. Tayeb, P. Sabouroux, N. Guerin and P. Vincent, *Phys Rev Lett*, 2002, **89**, 213902.
20. R. W. Ziolkowski, *Phys Rev E Stat Nonlin Soft Matter Phys*, 2004, **70**, 046608.
21. E. Sachet, *Transition Metal Oxides for Infrared Optoelectronics*, North Carolina State University, 2015.
22. F. Wooten, *Optical properties of solids*, Academic press, 2013.
23. E. Kretschmann and H. Raether, *Z Naturforsch a-Astrophys Phys Phys Chem*, 1968, **A 23**, 2135-&.
24. E. Kretschmann, *Optics Communications*, 1972, **5**, 331-336.
25. H. Raether, *Springer Tract Mod Phys*, 1988, **111**, 1-133.
26. A. Otto, *Z Phys*, 1968, **216**, 398-&.
27. J. M. Brockman, B. P. Nelson and R. M. Corn, *Ann Rev Phys Chem*, 2000, **51**, 41-63.
28. R. Karlsson, *J Mol Recognit*, 2004, **17**, 151-161.
29. A. C. Malmborg and C. A. K. Borrebaeck, *J Immun Meth*, 1995, **183**, 7-13.
30. J. M. McMahon, G. C. Schatz and S. K. Gray, *Phys Chem Chem Phys*, 2015, **17**, 19670-19671.
31. P. C. Wu, T. H. Kim, A. S. Brown, M. Losurdo, G. Bruno and H. O. Everitt, *Appl Phys Lett*, 2007, **90**.
32. E. J. Zeman and G. C. Schatz, *Journal of Physical Chemistry*, 1987, **91**, 634-643.
33. B. Cooper, H. Ehrenreich and H. Philipp, *Phys Rev*, 1965, **138**, A494.
34. H. Ehrenreich and H. Philipp, *Phys Rev*, 1962, **128**, 1622.
35. S. Franzen, *Journal of Physical Chemistry C*, 2008, **112**, 6027-6032.
36. A. G. Frutos, S. C. Weibel and R. M. Corn, *Analytical Chemistry*, 1999, **71**, 3935-3940.

37. B. P. Nelson, A. G. Frutos, J. M. Brockman and R. M. Corn, *Anal Chem*, 1999, **71**, 3928-3934.
38. P. Nyga, V. P. Drachev, M. D. Thoreson and V. M. Shalaev, *Applied Physics B*, 2008, **93**, 59-68.
39. G. V. Naik, V. M. Shalaev and A. Boltasseva, *Adv Mater*, 2013, **25**, 3264-3294.
40. G. V. Naik, J. Kim and A. Boltasseva, *Opt Mater Exp*, 2011, **1**, 1090-1099.
41. M. Z. Alam, I. De Leon and R. W. Boyd, *Science*, 2016, **352**, 795-797.
42. A. J. Haes and R. P. Van Duyne, *Anal Bioanal Chem*, 2004, **379**, 920-930.
43. N. D. Burrows, S. Harvey, F. A. Idesis and C. J. Murphy, *Langmuir*, 2017, **33**, 1891-1907.
44. J. Cao, T. Sun and K. T. V. Grattan, *Sens Act B-Chem*, 2014, **195**, 332-351.
45. B. Sharma, R. R. Frontiera, A. I. Henry, E. Ringe and R. P. Van Duyne, *Materials Today*, 2012, **15**, 16-25.
46. M. S. Kang, M. Losego, E. Sachet, J. P. Maria and S. Franzen, *Acs Phot*, 2016, **3**, 1993-1999.
47. A. Hryciw, Y. C. Jun and M. L. Brongersma, *Nat Mater*, 2010, **9**, 3-4.
48. R. Soref, *Nat Photon*, 2010, **4**, 495-497.
49. F. A. Trumbore, *Bell System Tech J*, 1960, **39**, 205-233.
50. J. W. Cleary, R. E. Peale, D. J. Shelton, G. D. Boreman, C. W. Smith, M. Ishigami, R. Soref, A. Drehman and W. R. Buchwald, *J Opt Soc Am B-Opt Phys*, 2010, **27**, 730-734.
51. K. Maex, *Mater Sci Eng R-Rep*, 1993, **11**, 53-153.
52. S. Maekawa, *J Phys Soc Jap*, 1962, **17**, 1592-&.
53. P. Biagioni, J. Frigerio, A. Samarelli, K. Gallacher, L. Baldassarre, E. Sakat, E. Calandrini, R. W. Millar, V. Giliberti, G. Isella, D. J. Paul and M. Ortolani, *J Nanophoto*, 2015, **9**.
54. J. Frigerio, A. Ballabio, G. Isella, E. Sakat, G. Pellegrini, P. Biagioni, M. Bollani, E. Napolitani, C. Manganelli, M. Virgilio, A. Grupp, M. P. Fischer, D. Brida, K. Gallacher, D. J. Paul, L. Baldassarre, P. Calvani, V. Giliberti, A. Nucara and M. Ortolani, *Phys Rev B*, 2016, **94**.
55. A. Samarelli, J. Frigerio, E. Sakat, L. Baldassarre, K. Gallacher, M. Finazzi, G. Isella, M. Ortolani, P. Biagioni and D. J. Paul, *Thin Solid Films*, 2016, **602**, 52-55.
56. S. Law, D. C. Adams, A. M. Taylor and D. Wasserman, *Opt Express*, 2012, **20**, 12155-12165.
57. G. Manna, R. Bose and N. Pradhan, *Angew Chem Int Ed Engl*, 2013, **52**, 6762-6766.
58. U. Guler, G. V. Naik, A. Boltasseva, V. M. Shalaev and A. V. Kildishev, *Appl Phys B-Laser Opt*, 2012, **107**, 285-291.
59. A. N. Grigorenko, M. Polini and K. S. Novoselov, *Nat Photon*, 2012, **6**, 749-758.
60. M. Jablan, H. Buljan and M. Soljacic, *Phys Rev B*, 2009, **80**.
61. T. Low and P. Avouris, *Acs Nano*, 2014, **8**, 1086-1101.
62. P. Tassin, T. Koschny, M. Kafesaki and C. M. Soukoulis, *Nat Photon*, 2012, **6**, 259-264.
63. S. K. V. Farahani, V. Munoz-Sanjose, J. Zuniga-Perez, C. F. McConville and T. D. Veal, *Applied Physics Letters*, 2013, **102**.
64. H. Yan, T. Low, W. Zhu, Y. Wu, M. Freitag, X. Li, F. Guinea, P. Avouris and F. Xia, *Nat Photon*, 2013, **7**, 394-399.
65. S. H. Brewer, D. A. Brown and S. Franzen, *Langmuir*, 2002, **18**, 6857-6865.
66. S. Moses, S. H. Brewer, S. Kraemer, R. R. Fuierer, L. B. Lowe, C. Agbasi, M. Sauthier and S. Franzen, *Sens Act B-Chem*, 2007, **125**, 574-580.
67. C. Rhodes, S. Franzen, J.-P. Maria, M. Losego, D. N. Leonard, B. Laughlin, G. Duscher and S. Weibel, *J Appl Phys*, 2006, **100**, 054905.
68. M. D. Losego, A. Y. Efremenko, C. L. Rhodes, M. G. Cerruti, S. Franzen and J. P. Maria, *J Appl Phys*, 2009, **106**.
69. M. Hiramatsu, K. Imaeda, N. Horio and M. Nawata, *J Vac Sci Tech A: Vac Surf Film*, 1998, **16**, 669-673.
70. H. Kim, M. Osofsky, S. M. Prokes, O. J. Glembocki and A. Piqué, *Appl Phys Lett*, 2013, **102**, 171103.

71. G. V. Naik and A. Boltasseva, *Metamat*, 2011, **5**, 1-7.
72. S. H. Brewer and S. Franzen, *Journal of Physical Chemistry B*, 2002, **106**, 12986-12992.
73. I. Hamberg, A. Hjortsberg and C. G. Granqvist, *Appl Phys Lett*, 1982, **40**, 362-364.
74. A. Hjortsberg, I. Hamberg and C. G. Granqvist, *Thin Solid Films*, 1982, **90**, 323-326.
75. B. G. Lewis and D. C. Paine, *Mrs Bulletin*, 2000, **25**, 22-27.
76. P. M. Armistead and H. H. Thorp, *Anal Chem*, 2001, **73**, 558-564.
77. S. R. VanderKam, E. S. Gawalt, J. Schwartz and L. B. Bocarsly, *Langmuir*, 1999, **15**, 6598-6600.
78. P. M. Armistead and H. H. Thorp, *Anal Chem*, 2000, **72**, 3764-3770.
79. D. Kim and S. Kim, *Thin Solid Films*, 2002, **408**, 218-222.
80. S. Y. Oh and S. H. Han, *Langmuir*, 2000, **16**, 6777-6779.
81. M. Tamada, H. Koshikawa, F. Hosoi and T. Suwa, *Thin Solid Films*, 1998, **315**, 40-43.
82. S. H. Brewer, D. Wicaksana, J. P. Maria, A. I. Kingon and S. Franzen, *Chem Phys*, 2005, **313**, 25-31.
83. F. Abeles, *J Opt Soc Am*, 1957, **47**, 473-482.
84. D. W. Berreman, *Phys. Rev.*, 1963, **130**, 2193-2198.
85. B. Harbecke, B. Heinz and P. Grosse, *Appl. Phys. A*, 1985, **38**, 263-267.
86. M. Kanehara, H. Koike, T. Yoshinaga and T. Teranishi, *J Am Chem Soc*, 2009, **131**, 17736-17737.
87. S. Szunerits and R. Boukherroub, *Introduction to Plasmonics: Advances and Applications*, Pan Stanford, 2015.
88. X. G. Liu, J. H. Kang, H. T. Yuan, J. Park, Y. Cui, H. Y. Hwang and M. L. Brongersma, *Acs Photonics*, 2018, **5**, 1493-1498.
89. S. C. Kehr, Y. M. Liu, L. W. Martin, P. Yu, M. Gajek, S. Y. Yang, C. H. Yang, M. T. Wenzel, R. Jacob, H. G. von Ribbeck, M. Helm, X. Zhang, L. M. Eng and R. Ramesh, *Nat Commun*, 2011, **2**, 249.
90. Y. J. Zhong, S. D. Malagari, T. Hamilton and D. Wasserman, *J Nanophoton*, 2015, **9**.
91. Z. Lu, X. Pan, Y. Ma, Y. Li, L. Zheng, D. Zhang, Q. Xu, Z. Chen, S. Wang, B. Qu, F. Liu, Y. Huang, L. Xiao and Q. Gong, *RSC Adv.*, 2015, **5**, 11175-11179.
92. L. Yue, B. Yan, M. Attridge and Z. Wang, *Sol Ener*, 2016, **124**, 143-152.
93. F. P. Koffyberg, *Phys Lett A*, 1969, **A 30**, 37-&.
94. R. D. Shannon, *Acta Crystallographica Section A*, 1976, **32**, 751-767.
95. E. Runnerstrom, K. Kelley, E. Sachet, C. T. Shelton and J. P. Maria, *Acs Phot*, 2017, **4**, 1885-1892.
96. K. Kelley, E. Sachet, C. T. Shelton and J. P. Maria, *APL Mater*, 2017, **5**, 076105.
97. G. Mie, *Annal Phys*, 1908, **25**, 377-445.
98. G. Bühler, D. Thölmann and C. Feldmann, *Advanced Materials*, 2007, **19**, 2224-2227.
99. R. A. Gilstrap, C. J. Capozzi, C. G. Carson, R. A. Gerhardt and C. J. Summers, *Advanced Materials*, 2008, DOI: 10.1002/adma.200702556, NA-NA.
100. E. L. Runnerstrom, A. Bergerud, A. Agrawal, R. W. Johns, C. J. Dahlman, A. Singh, S. M. Selbach and D. J. Milliron, *Nano Lett*, 2016, **16**, 3390-3398.
101. J. A. Faucheaux, A. L. Stanton and P. K. Jain, *J Phys Chem Lett*, 2014, **5**, 976-985.
102. X. Liu, L. Li, Y. Yang, Y. Yin and C. Gao, *Nanoscale*, 2014, **6**, 4513-4516.
103. X.-Y. Zhang, F. Shan, H.-L. Zhou, D. Su, X.-M. Xue, J.-Y. Wu, Y.-Z. Chen, N. Zhao and T. Zhang, *Journal of Materials Chemistry C*, 2018, **6**, 989-999.
104. V. Giannini, Y. Zhang, M. Forcales and J. G. Rivas, *Optical Society of America*, 2008, **16**.
105. A. Agrawal, A. Singh, S. Yazdi, A. Singh, G. K. Ong, K. Bustillo, R. W. Johns, E. Ringe and D. J. Milliron, *Nano Lett*, 2017, **17**, 2611-2620.
106. R. Buonsanti, A. Llordes, S. Aloni, B. A. Helms and D. J. Milliron, *Nano Lett*, 2011, **11**, 4706-4710.
107. M. Yan, M. Lane, C. R. Kannewurf and R. P. H. Chang, *Appl Phys Lett*, 2001, **78**, 2342-2344.
108. T. R. Gordon, T. Paik, D. R. Klein, G. V. Naik, H. Caglayan, A. Boltasseva and C. B. Murray, *Nano Lett*, 2013, **13**, 2857-2863.
109. A. Agrawal, I. Kriegel and D. J. Milliron, *J Phys Chem C*, 2015, **119**, 6227-6238.

110. D. G. Brookins, *Chem Geol*, 1986, **54**, 271-278.
111. M. Pourbaix, *Atlas of electrochemical equilibria in aqueous solutions*, Pergamon Press, Oxford; New York, 1966.
112. T. W. Ebbesen, *Acc Chem Res*, 2016, **49**, 2403-2412.
113. P. Torma and W. L. Barnes, *Rep Prog Phys*, 2015, **78**, 013901.
114. H. A. Atwater and A. Polman, *Nat Mater*, 2010, **9**, 205-213.
115. K. Tvingstedt, N.-K. Persson, O. Inganäs, A. Rahachou and I. V. Zozoulenko, *Applied Physics Letters*, 2007, **91**.
116. S. Lal, S. Link and N. Halas, *Nature*, 2007, **1**, 641-648.
117. N. L. A. Melikyan, S. Walheim, P. M. Leufke, S. Ulrich, J. Ye, P. Vincze, H. Hahn, Th. Schimmel, C. Koos, W. Freude, and J. Leuthold, *Optical Society of America* 2011, **19**, 8855-8869.
118. M. Hill, M. Marell, E. Leong, B. Smalbrugge, Y. Zhu, M. Sun, P. Veldhoven, E. Geluk, F. Karouta, Y. Oei, R. Notzel, C. Ning and M. Smit, *Optical Society of America* 2009, **17**, 11107-11112.
119. J. Dionne, K. Diest, L. Sweatlock and H. Atwater, *Nano Letters*, 2009, **9**, 897-902.
120. A. V. Krasavin and A. V. Zayats, *Phys Rev Lett*, 2012, **109**, 053901.

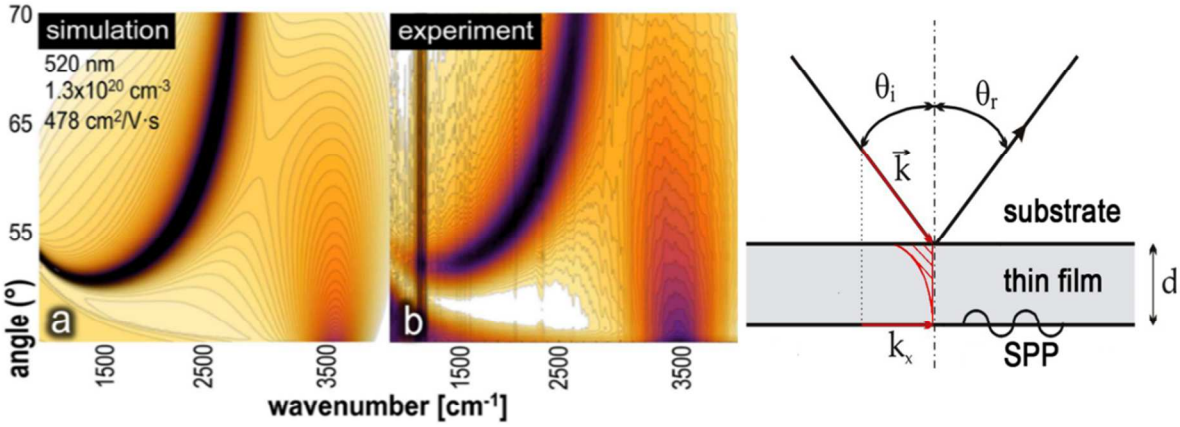

Review of material properties of conducting metal oxides that make them suitable for mid-infrared surface plasmon resonance applications.